Journal of ELECTRONIC MATERIALS, Vol. 41, No. 6, 2012
DOI: 10.1007/s11664-012-2047-0

Thin-Film Thermoelectric Modules for Power Generation Using Focused Solar Light

MIZUE MIZOSHIRI,[1,2] MASASHI MIKAMI,[1] KIMIHIRO OZAKI,[1] and KEIZO KOBAYASHI[1]

1.—National Institute of Advanced Industrial Science and Technology (AIST), 2266-98, Anagahora, Shimoshidami, Moriyama, Nagoya 463-8560, Japan. 2.—e-mail: mizoshiri-mizue@aist.go.jp

We demonstrated the fabrication of thin-film thermoelectric generators and evaluated their generation properties using solar light as a thermal source. Thin-film elements of $Bi_{0.5}Sb_{1.5}Te_3$ (*p*-type) and $Bi_2Te_{2.7}Se_{0.3}$ (*n*-type), which were patterned using the lift-off technique, were deposited on glass substrates using radiofrequency magnetron sputtering. After annealing at 300°C, the average Seebeck coefficients of *p*- and *n*-type films were 150 μV/K and −104 μV/K, respectively, at 50°C to 75°C. A cylindrical lens was used to focus solar light to a line shape onto the hot side of the thin-film thermoelectric module with 15 *p*–*n* junctions. The minimum width of line-shaped solar light was 0.8 mm with solar concentration of 12.5 suns. We studied the properties of thermoelectric modules with different-sized *p*–*n* junctions on the hot side, and obtained maximum open voltage and power values of 140 mV and 0.7 μW, respectively, for a module with 0.5-mm *p*–*n* junctions. The conversion efficiency was 8.75×10^{-4}%, which was approximately equal to the value estimated by the finite-element method.

Key words: Thermoelectric generator, thin-film thermoelectric module, lithography, solar

INTRODUCTION

Small-scale energy-harvesting devices have received attention as power supply devices for wireless sensors and/or microscale devices. These devices convert natural or waste energy in the environment, such as light, vibration, and thermal energy, to electric energy.[1,2] Thermoelectric generation is a promising candidate to convert a temperature gradient, generated by thermal energy, directly to electric energy. In particular, thin-film thermoelectric generators (TEGs) are expected to be used in various applications because of their high integration of two-dimensional thermoelectric elements. By connecting a number of thermoelectric elements serially, it is possible to obtain a relatively high voltage of approximately 1 V using thin-film TEGs.[3] Consequently, the power generated can be charged to batteries, integrated with the thin-film TEGs. Thin-film TEGs have been reported to be used for low-power consumption devices in the microwatt range.[4–6] Bi-Te material thin films, which are used for thin-film TEGs because of their excellent figures of merit in low temperature ranges, have been deposited by sputtering,[4] the flash evaporation method,[5] and metalorganic chemical vapor deposition.[6] The conversion efficiency of thermoelectric generation is generally lower than that of photovoltaic conversion. However, thermoelectric conversion presents the important advantage that light in a broad sense, such as solar light and/or infrared thermal radiation, is used as thermal energy for conversion to electric energy, whereas the wavelengths of light available for photovoltaic conversion depend on the bandgaps of the photovoltaic materials; for example, because of the large bandgaps, amorphous silicon photovoltaic solar cells cannot

(Received July 15, 2011; accepted March 2, 2012; published online April 3, 2012)

convert near-infrared light, which accounts for 40% of solar light.[7]

In general, the conversion efficiency of thin-film TEGs is lower than that of bulk TEGs because of heat loss. However, thin-film TEGs present two important advantages. First, they have high portability and integration. Compared with bulk TEGs, thin-film TEGs with numerous thermoelectric elements can be fabricated easily using microelectromechanical systems (MEMS) processes, such as lithography and lift-off processes, which are well established for highly reliable, large-area microfabrication. Also, thin-film TEGs are useful for small-scale energy-harvesting devices because of their high generation voltage. The total energy available for the system decreases as the size of the lens decreases because of the reduction of its incident area. When the total energy is small, the hot sides of TEGs with small thermal resistance, such as bulk TEGs, cannot be heated sufficiently. Therefore, thin-film TEGs with large thermal resistances are useful for generating large temperature differences.

To generate sufficient temperature differences between the hot and cold sides of TEGs using low-power light such as solar light and infrared thermal radiation, concentration of the light is effective. In case of large-scale solar TEGs with bulk thermoelectric modules, concentrators, such as large-scale lenses and parabolas, have been used to generate a temperature gradient between the hot and cold sides of the modules.[8,9] Furthermore, TEGs with high conversion efficiency have been achieved by optimizing the solar light absorber and heat transfer of systems.[10]

In this study, as a first step to develop thin-film TEGs using light with low radiation flux such as solar light and infrared thermal radiation, thin-film TEGs using focused solar light as a heat source were proposed. Prototype TEGs with simple structures were designed and fabricated. The thin-film TEGs were evaluated using a solar simulator.

DEVICE DESIGN AND SIMULATION

Figure 1 shows a schematic illustration of the thin-film thermoelectric module. The thin-film module is formed on an 18 mm × 18 mm glass substrate with 150 μm thickness. Solar light is focused by a cylindrical lens to a line shape onto the hot side of the thin-film thermoelectric module with 15 p–n junctions. The radius of curvature, width, and length of the cylindrical lens were 7.75 mm, 10 mm, and 20 mm, respectively. Considering the wavelength dependence of the refractive index and spherical aberration of the lens, the width of the focused solar light was calculated as 0.8 mm (12.5 suns). The solar light was focused ~12.5× because a lens with short working distance can be used with thin-film TEGs with two-dimensional structure. The cold sides of the p–n junctions were parallel to the two sides of a hot side, as presented in Fig. 1. The length, width, and thickness of the thin-film thermoelectric elements were 5 mm, 250 μm, and 1 μm, respectively. Following the deposition of SiO_2 as insulator thin film on the thin-film modules, a solar light absorber of carbon thin film was patterned on the p–n junctions above the hot side. The thickness, width, and length of the carbon thin film were 6 μm, 1 mm, and 18 mm, respectively. The absorber thickness was sufficient to neglect the light transmittance. Cu bulk chips (6 mm × 2 mm × 18 mm) were placed beyond the p–n junctions of the cold sides as heat sinks. Considering the solar flux as 100 mW/cm^2 and the lens transmittance as 96%, the heat flux of the focused solar light was calculated as 1200 mW/cm^2.

The temperature distribution of the thermoelectric modules was estimated using the finite-element method (FEM, Multiphysics v4.1; Comsol Inc.). Figure 2a presents a cross-section of the calculation model. The thickness of the glass substrate was 150 times greater than that of the thermoelectric thin films. In contrast, the thermal conductivities of the glass substrate and thermoelectric thin films were approximately equal (ca. 1.5 W/mK).[9] Consequently, the temperature distribution of the glass substrate was calculated as the module temperature distribution, assuming that the thermal conductivity of the thin films can be considered negligibly small compared with that of the entire thermoelectric module. Calculation parameters such as material properties are presented in Table I. In the FEM simulation, the heat transfer coefficient between the system and the ambient air was assumed to be 10 W/m^2 K as a common value. The maximum and minimum sizes of the mesh were 5×10^{-3} m and 1×10^{-6} m, respectively. These values were confirmed to be sufficiently small that the temperature distribution was not affected. The temperature distribution on the cross-section of the modules is presented in Fig. 2b. The maximum surface temperature was calculated as 78°C at the module center. The cold sides of the p–n junctions were formed on the surface, 5 mm from the center of the modules; at this distance the temperature was almost equal to that at the substrate edge. The open

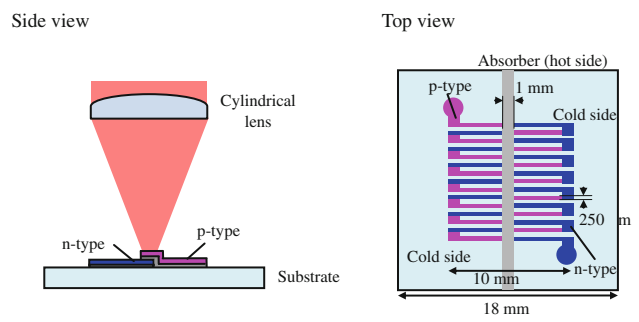

Fig. 1. Schematic illustration of thermoelectric modules used for focused solar light.

Table I. Material properties used in FEM simulation

	Thermal Conductivity (W/mK)	Heat Capacity (J/kg K)	Density (kg/m^3)
Module substrate (SiO_2)	1.38	703	2203
Fin (Cu)	400	385	8700
Absorber (carbon)	140	710	2000

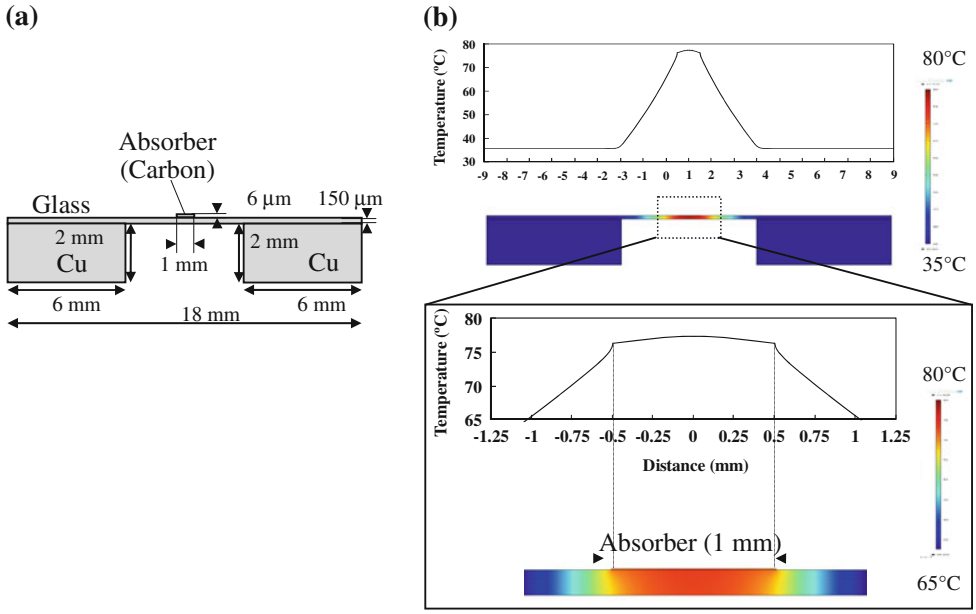

Fig. 2. Cross-section of (a) calculation model and (b) temperature distribution of thin-film thermoelectric modules by FEM simulation.

voltages depended on the temperature differences between the borders of the *p*–*n* junctions on the hot and cold sides because the thermoelectric power inside the *p*–*n* junctions was canceled. When the lengths of *p*–*n* junctions on the hot sides were 0.5 mm and 1 mm, the temperature differences between the hot and cold sides were approximately equal, i.e., 42°C and 41°C, respectively. The temperature difference was estimated as 30°C when the *p*–*n* junction length was 2 mm. For this study, we prepared three types of thin-film thermoelectric modules with *p*–*n* junction lengths on the hot side of 0.5 mm, 1 mm, and 2 mm. Subsequently, we evaluated their generation properties.

DEVICE FABRICATION

Thermoelectric Film Deposition

P- and *n*-type thermoelectric thin films of $Bi_{0.5}Sb_{1.5}Te_3$ and $Bi_2Te_{2.7}Se_{0.3}$, which have excellent thermoelectric properties such as large figures of merit in the low temperature range, were used.[4] These thin films can be deposited using common deposition methods used in MEMS processes such as sputtering and evaporation. The thin films were deposited by radiofrequency (RF) magnetron sputtering. The RF power, operating pressure, and substrate temperature were 30 W, 1 Pa, and 100°C, respectively. The substrates were heated to remove surface contamination, such as developer or rinse water that survived the lithographic process for resist patterning. The deposition rates of the *p*- and *n*-type thermoelectric thin films were 110 nm/min and 90 nm/min, respectively. The deposited thin films were annealed at 300°C for 1 h to crystalline order. Figure 3 shows x-ray diffraction patterns of the as-deposited and annealed thermoelectric thin films. The thermoelectric thin films were crystallized by annealing. The x-ray intensity ratios $I_{(006)}/I_{(015)}$ of the *p*- and *n*-type thermoelectric thin films were much lower than 0.5, i.e., 0.007 and 0.006, respectively. This result suggests that, because the thin films were deposited on glass substrate,[11] the thermoelectric thin films were not oriented in the direction of the *c*-axis.[12] Figure 4 shows the temperature dependencies of the Seebeck coefficients. The average Seebeck coefficients of the *p*- and *n*-type films at 50°C to 75°C were 150 μV/K and -104 μV/K, respectively. The module surface temperatures were calculated using FEM simulation. The electric conductivities of the *p*- and *n*-type

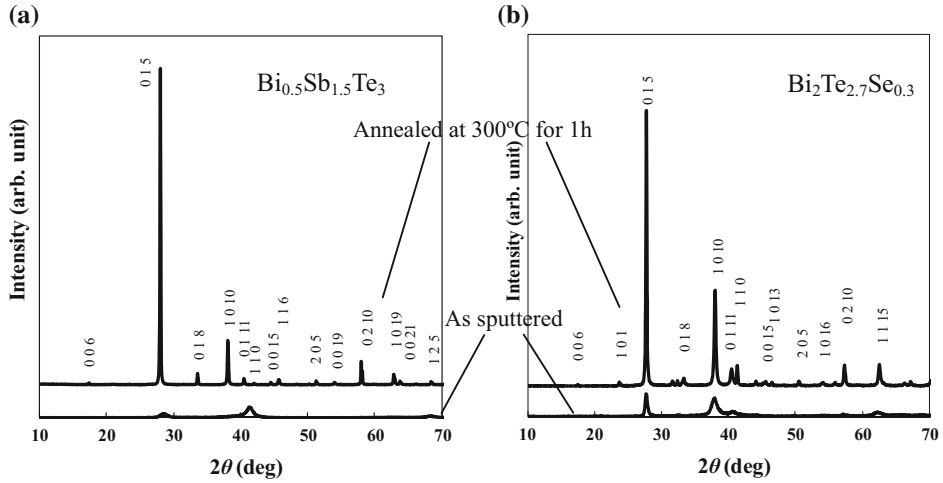

Fig. 3. X-ray diffraction patterns of (a) $Bi_{0.5}Sb_{1.5}Te_3$ (*p*-type) and (b) $Bi_2Te_{2.7}Se_{0.3}$ (*n*-type) thin films.

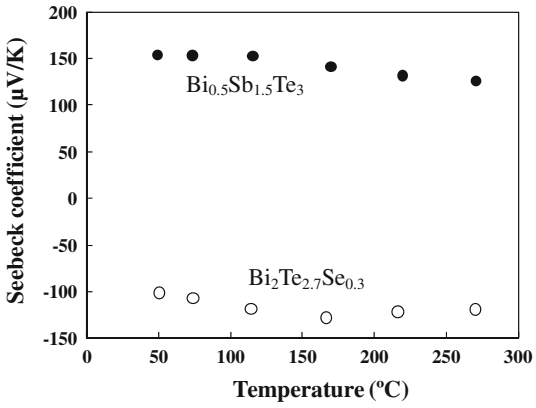

Fig. 4. Seebeck coefficients of $Bi_{0.5}Sb_{1.5}Te_3$ (*p*-type) and $Bi_2Te_{2.7}Se_{0.3}$ (*n*-type) thin films.

thermoelectric thin films were 1400 S/cm and 1800 S/cm, respectively, at ca. 75°C.

The temperature difference determines the open voltage and generation power of the modules. The open voltage V_0 and the maximum power of modules can be expressed, respectively, as Eqs. 1 and 2.

$$V_0 = (S_p - S_n) \cdot \Delta T \cdot N, \tag{1}$$

$$P = V_0^2 R / (R_{\text{module}} + R)^2, \tag{2}$$

where S_p and S_n denote the *p*- and *n*-type Seebeck coefficients, ΔT is the temperature difference between the hot and cold sides of *p*–*n* junctions, N is the number of pairs of *p*–*n* junctions, R is the load resistance, and R_{module} is the module resistance. The temperature gradient was generated from the center of the glass substrate surface to both sides of the edges, as presented in Fig. 2b. Temperature differences between the hot and cold sides of the *p*–*n* junctions increased concomitantly with decreasing lengths of *p*–*n* junctions on the hot side. Consequently, large open voltages were expected to be obtained by decreasing the lengths of the *p*–*n* junctions in Eq. 1. Moreover, the difference of electric resistance between these modules could be neglected because the length of a pair of thin-film thermoelectric elements (10 mm) was much greater than those of the *p*–*n* junctions on the hot side when the lengths of the *p*–*n* junctions were 0.5 mm, 1 mm, and 2 mm. Therefore, module powers were also expected to increase with decreasing lengths of *p*–*n* junctions in Eq. 2.

Fabrication Process

Figure 5 presents fabrication processes for thin-film thermoelectric modules. MEMS processes, such as photolithography and the lift-off technique, were used to pattern the thin-film thermoelectric elements. First, a chemically amplified positive-tone photoresist (PMER P-CA1000PM; Tokyo Ohka Kogyo Co. Ltd.) was spin-coated onto glass substrates. Then, ultraviolet (UV) light was irradiated through photomasks. As the lift-off process was used for thin-film patterning, the resist thickness was as high as 13 μm. Prebaking and postexposure baking were conducted at 130°C for 6 min and 76°C for 6 min, respectively. After development, *n*-type thermoelectric thin films were deposited using resist patterns as masks. Subsequently, the resist masks were removed. To form *p*-type thin-film thermoelectric elements, the resist was spin-coated and exposed to UV light. After development, *p*-type thermoelectric thin films were deposited using resist patterns as masks. During the lift-off process, the adhesion between the thermoelectric thin films and glass substrates was low, and the films broke away from the substrate. Consequently, a buffered layer of Cr thin films with 1 nm thickness was deposited between the thermoelectric thin films and the substrates. Under this condition, the electric

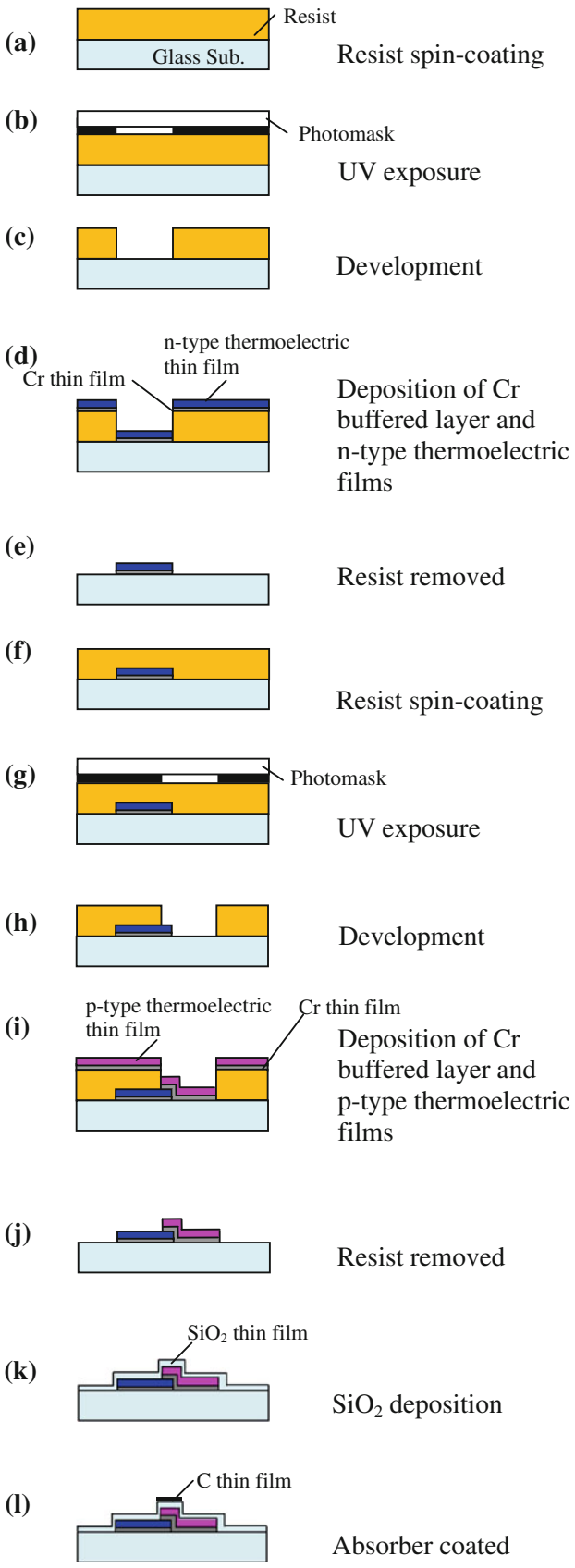

Fig. 5. Thermoelectric module fabrication process.

resistance ratio of thermoelectric to Cr thin films was approximately 10^{-4}, which was expected to be negligible for the module properties. After patterning the thermoelectric thin films on substrates, they were annealed for crystalline ordering. Then, SiO_2 thin films of 500 nm thickness were deposited on the thin-film modules as insulators. Carbon thin films were formed as line-shaped structures above the hot sides of the *p–n* junctions.

EXPERIMENTAL RESULTS AND DISCUSSION

Figure 6 shows the thin-film thermoelectric module. Thin-film thermoelectric patterns were formed without film separation from the substrate. The electric resistance of the module was 6.93 kΩ when the *p–n* junctions on the hot sides were 0.5 mm. This value was 76% larger than the value of 3.94 kΩ calculated using the electric conductivities of the thermoelectric thin films. It was assumed that the contact resistances, such as *p–n* junctions including Cr buffered layers of the modules, increased the module resistance. We used the same fabrication process to prepare thin-film thermoelectric modules with 1-mm and 2-mm *p–n* junctions on the hot sides.

The power generation properties of the thin-film thermoelectric modules were evaluated using a solar simulator (model 10500, AM1.5G; ABET Technologies, Inc.). Collimated light of 100 mW/cm^2 was irradiated vertically onto the cylindrical lenses. Figure 7 presents the solar simulator irradiation and the thermal image. The module was heated mainly at a focused line of solar light. However, the cold sides of the *p–n* junctions were not heated. Temperature differences between the hot and cold sides of the *p–n* junctions of approximately 40°C were generated, judging from the thermal image presented in Fig. 7. Power generation properties of thin-film thermoelectric modules are presented in Fig. 8 for *p–n* junctions of 0.5 mm, 1 mm, and 2 mm on the hot sides. When the maximum open voltage and power were obtained, the *p–n* junctions were 0.5 mm. The open voltage and power were 140 mV

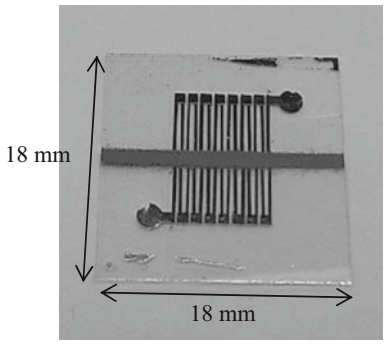

Fig. 6. Thin-film thermoelectric module.

and 0.7 μW, respectively. The conversion efficiency was 8.75×10^{-4}%.

Considering the FEM simulation results, the thermoelectric modules had a temperature gradient from the hot sides to either cold side. Consequently, the temperature difference between the hot and cold sides of the *p–n* junctions was expected to increase as the length of the *p–n* junctions decreased. The maximum open voltage and power were obtained in the module with 0.5-mm, 1-mm, and 2-mm *p–n* junctions. These experimental results were qualitatively consistent with the expectation described above. The temperature difference in the module with 0.5-mm *p–n* junctions was estimated as 40°C, using the value of the experimentally obtained open voltage and Eq. 1. This value is almost equal to that obtained in the simulation. However, the temperature differences of the modules with 1-mm and 2-mm *p–n* junctions were smaller than those estimated by the FEM simulations. In those simulations, the heat flux was assumed to be constant across the line shape of 0.8 mm width, which was an ideal condition without considering the intensity distribution due to lens focusing. However, when solar light is experimentally focused using a cylindrical lens, the heat flux is expected to show a distribution around the borders of the focused area because chromatic and spherical aberrations generate a gradient in the light intensity distribution from the center to the edges of the absorber. Namely, the solar flux at the absorber edges will be lower than that at the absorber center. Moreover, heat radiation losses from the absorber increase with decreasing incident solar flux.[10] Our experimental results showed that differences between the open voltage values and those estimated using FEM increased concomitantly with the length of the *p–n* junctions on the hot side. This result can be explained by heat radiation losses from the absorber. The conversion efficiency of 8.75×10^{-4}% remained small because solar light was roughly focused to a line shape. The heat radiation losses from the solar absorber were still large. However, the radiation losses in the focused light are expected to be lower when using an optical concentrator to spot-focus the light.

As a first step to achieve thin-film TEGs with a small concentrator, carbon thin film was used as the solar absorber to roughly focus the solar light. The feasibility of thin-film TEGs using light with low radiation flux as thermal energy was proved in this study. Optimization of the solar absorber is expected to improve the optothermal conversion of the light using a wavelength-selective solar absorber.

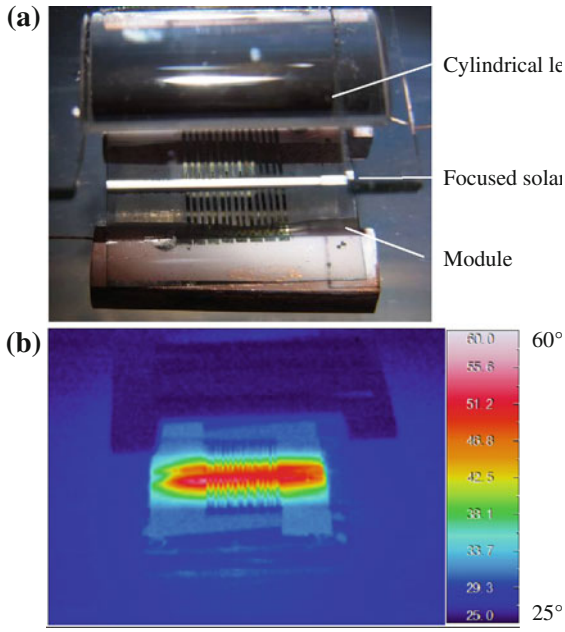

Fig. 7. (a) Photograph and (b) thermal image of thin-film thermoelectric modules irradiated by focused solar light using a cylindrical lens.

CONCLUSIONS

We demonstrated fabrication of TEGs and evaluated their generation properties using solar light as a thermal source. The maximum open voltage and power, as obtained using the module with 0.5 mm-*p–n* junctions, were 140 mV and 0.7 μW, respectively. The conversion efficiency was 8.75×10^{-4}%, approximately equal to the value estimated by FEM. The results demonstrate the feasibility of a

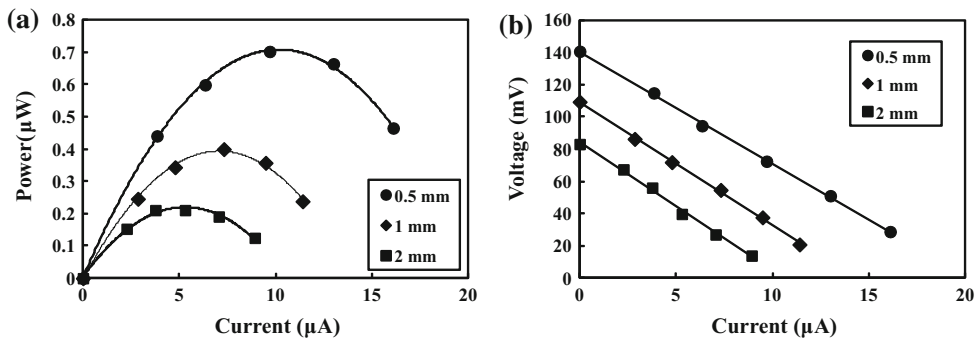

Fig. 8. (a) *I–V* and (b) *I–P* properties of thin-film thermoelectric modules irradiated by focused solar light using a cylindrical lens.

TEG that uses a small amount of focused light energy with low radiation flux. Future studies will yield greater generated power through optimization of the module design, such as the thickness of the thermoelectric thin films and the light absorber.

REFERENCES

1. N.S. Hudak and G.G. Amatucci, *J. Appl. Phys.* 103, 101301 (2008).
2. E.O. Torres and G.A. Rincon-Mara, *J. Energy Eng.* 134, 121 (2008).
3. J. Weber, K. Potje-Kamloth, F. Haase, P. Detemple, F. Völklein, and T. Doll, *Sens. Actuators* A132, 325 (2006).
4. G.J. Snyder, J.R. Lim, C.-K. Huang, and J.-P. Fleurial, *Nat. Mater.* 2, 528 (2003).
5. M. Takahashi, T. Shirakawa, K. Miyazaki, and H. Tsukamoto, *Sens. Actuators A Phys.* 138, 329 (2007).
6. S.-D. Kwon, B.-K. Ju, S.-J. Yoon, and J.-S. Kim, *J. Electron. Mater.* 38, 920 (2009).
7. E. Skoplaki and J.A. Palyvos, *Sol. Energy* 83, 614 (2009).
8. R. Amatya and R.J. Ram, *J. Electron. Mater.* 39, 1735 (2010).
9. P. Li, L. Cai, P. Zhai, X. Tang, Q. Zhang, and M. Niino, *J. Electron. Mater.* 39, 1522 (2010).
10. D. Kraemer, B. Poudel, H.-P. Feng, J.C. Caylor, B. Yu, X. Yan, Y. Ma, X. Wang, D. Wang, A. Muto, K. MacEnanery, M. Chiesa, Z. Ren, and G. Chen, *Nat. Mater.* 10, 532 (2011).
11. D. Bourgault, C.G. Garampon, N. Caillault, L. Carbone, and J.A. Aymami, *Thin Solid Films* 516, 8579 (2008).
12. I. Yashima, T. Sato, and Y. Toshio, *J. Jpn. Ceram. Soc.* 105, 152 (1997).